Observations of infragravity waves at the Monterey ocean bottom broadband station (MOBB)

David Dolenc and Barbara Romanowicz

Seismological Laboratory, University of California, 215 McCone Hall, #4760, Berkeley, California 94720, USA (dolenc@seismo.berkeley.edu)

Debra Stakes and Paul McGill

Monterey Bay Aquarium Research Institute, 7700 Sandholdt Road, Moss Landing, California 95039, USA

Doug Neuhauser

Seismological Laboratory, University of California, 215 McCone Hall, #4760, Berkeley, California 94720, USA

[1] Infragravity waves can be observed at the 1000 m deep ocean bottom broadband seismic station MOBB on stormy as well as quiet days. When compared to the energy of the short-period ocean waves recorded at the local buoys, infragravity waves in the longer than 20 s period band are found to be mainly locally generated from shorter-period waves. Two types of modulation of the infragravity signal are observed. First, the entire infragravity band signal is modulated in-phase with tides, possibly as a result of the nonlinear exchange of energy between the short-period waves and tidal currents. Second, a longer-period modulation of the infragravity signal is observed and is best correlated with the energy of the 14 s period ocean waves. This correlation indicates that the mechanism of generation of double frequency microseisms and infragravity waves are likely strongly related. Previously recorded data during the Oregon ULF/VLF experiment at 600 m water depth also indicate that infragravity waves are primarily locally generated.

1. Introduction

[2] The Monterey ocean bottom broadband station (MOBB) is a collaborative effort between the Monterey Bay Aquarium Research Institute (MBARI) and the Berkeley Seismological Laboratory (BSL). The MOBB was installed in April 2002, 40 km offshore in the Monterey Bay, at a water depth of 1000 m [*McGill et al.*, 2002; *Uhrhammer et al.*, 2002; *Romanowicz et al.*, 2003, 2005]. It is located west of the San Gregorio Fault, one of the major, yet not well documented faults of the San Andreas Fault System (Figure 1). The region is characterized by a very diverse topography; a wide, gently sloping continental shelf is found to the north, 1500 m deep Monterey Canyon is just south of MOBB, and a narrow shelf is present in Monterey Bay and further to the south. The MOBB is a continuously operated broadband seismic station and is considered the first step toward extending the Berkeley Digital Seismic Network (BDSN) westward of the Pacific-North America plate boundary. It follows
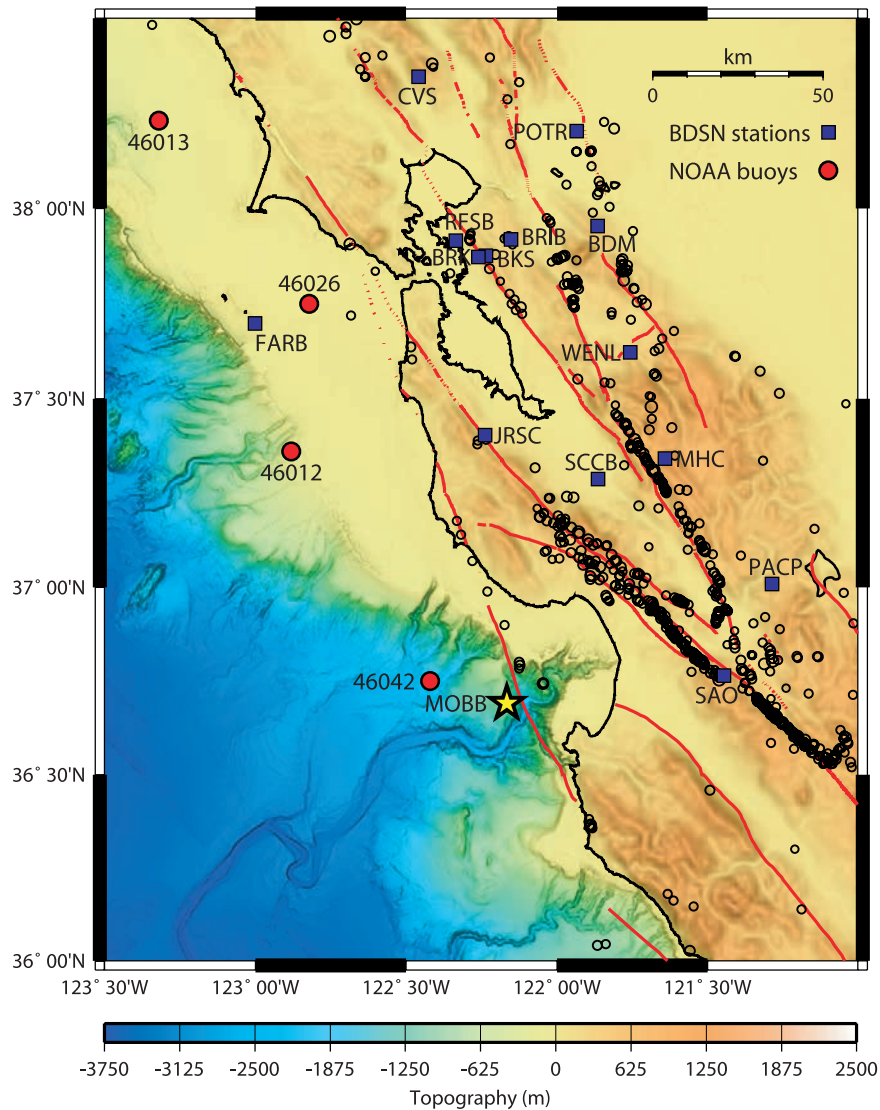
Figure 1. Locations of the MOBB (yellow) and the BDSN seismic stations (blue) shown against the seafloor and land topography. Background seismicity (ANSS catalog, 1968–2004, M3.5+) is shown in black. Locations of the NOAA buoys closest to the MOBB are shown in red. Fault lines from the California Division of Mines and Geology database are shown in red as well.

from the experience gained previously during the 3-monthlong MOISE deployment in 1997, which was located about 10 km to the west [*Romanowicz et al.*, 1998; *Stutzmann et al.*, 2001].

[3] The MOBB comprises a 3-component Guralp CMG-1T broadband seismometer buried in the ocean floor, a recording and battery package, as well as a collocated differential pressure gauge (DPG) [*Cox et al.*, 1984] and current meter, which measures ocean bottom current speed and direction [*Romanowicz et al.*, 2005]. At present, the station is autonomous and the data are on average retrieved every three months using the MBARI's remotely

operated vehicle *Ventana*. With a planned connection to the MARS (Monterey Accelerated Research System; http://www.mbari.org/mars) fiber-optic cable, the data will be retrieved continuously and in real-time and will be publicly available from the Northern California Earthquake Data Center (NCEDC; http://quake.geo.berkeley.edu/ncedc).

[4] The MOBB as well as future BDSN ocean bottom stations will enable us to better determine locations and mechanisms of offshore earthquakes, to learn more about the crustal structure at the continental edge, as well as to better understand the
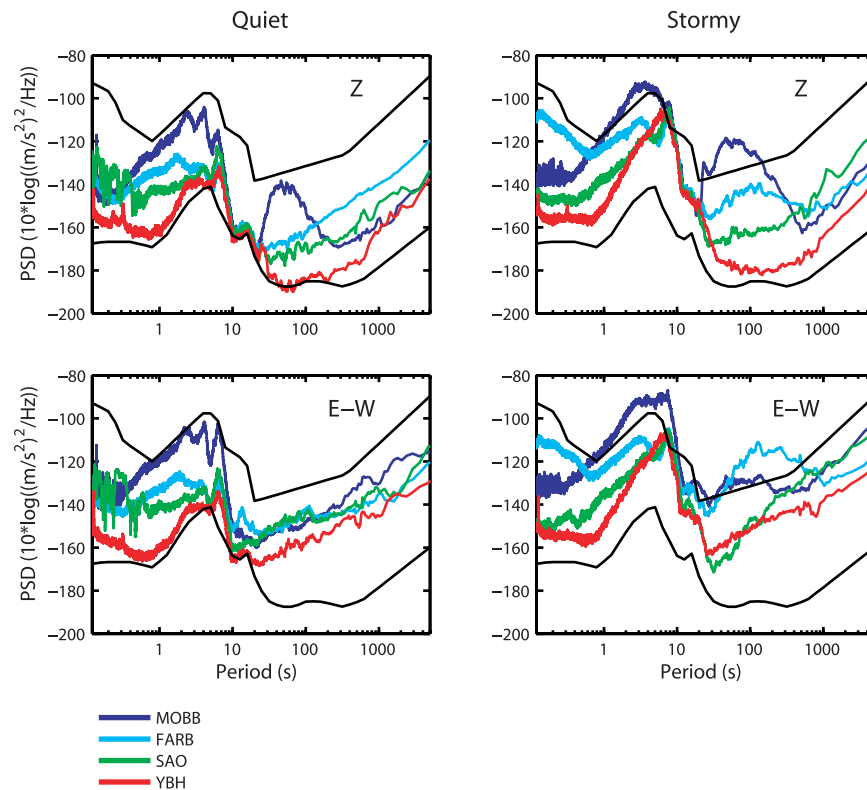
Figure 2. Comparison of the power spectral density (PSD) at the stations MOBB, FARB, SAO, and YBH calculated for a quiet day (2002, day 143) and for a stormy day (2002, day 350). Results obtained for the vertical (top) and for the horizontal components (E-W, bottom) are shown. The USGS high- and low-noise models for land stations are shown in black [*Peterson*, 1993].

plate-boundary processes and therefore better constrain the seismic hazard along the west coast of northern California. At the same time such permanent ocean bottom stations equipped with broadband seismometers will provide us new information on the coupling between the ocean and the solid earth.

[5] The broadband seismometer installed at MOBB is sensitive over a wide frequency range, from 50 Hz to 2.8 mHz (360 s). This enabled us to also observe the long-period signal which is largely due to the ocean surface infragravity waves.

2. Infragravity Waves

[6] Infragravity waves are ocean surface waves with periods longer than the wind-driven waves and the swell. Their wave amplitudes in the deep water are small (<1 cm) and they can be observed in the frequency band from 0.002 to 0.05 Hz. They were first observed near the shore by *Munk* [1949] and *Tucker* [1950]. The pressure fluctuations from infragravity waves at the deep seafloor were first measured by *Sutton et al.* [1965], and they were

first observed at the sea surface in the open ocean by *Snodgrass et al.* [1966]. Although high correlations have been observed between infragravity and shorter-period ocean waves (wind waves and swell) energy [e.g., *Munk*, 1949; *Tucker*, 1950; *Elgar et al.*, 1992; *Herbers et al.*, 1995a], the precise generation mechanism for infragravity waves is still not completely understood.

[7] In oceanography, infragravity waves are considered important for harbor oscillations and nearshore processes, such as sediment transport. In seismology, pressure fluctuations due to infragravity waves have been identified as an important source of long-period noise at the ocean bottom [*Webb et al.*, 1991; *Webb*, 1998]. Infragravity waves have recently also been proposed as a source of the Earth's continuous free oscillations [*Rhie and Romanowicz*, 2004; *Tanimoto*, 2005].

3. Power Spectral Density

[8] We first compared the power spectral density (PSD) at MOBB and three other stations of the BDSN network (Figure 2). Station SAO is the
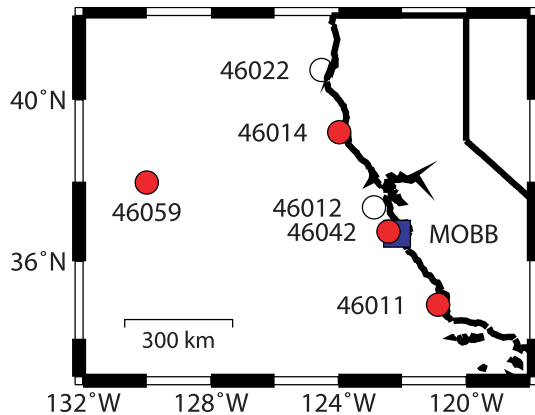
Figure 3. The location of some of the NOAA buoys closest to the MOBB. Red color indicates buoys with data available for the time period presented in Figure 4.

closest land station (see Figure 1), and station YBH is one of the quietest BDSN stations, located 560 km north of MOBB. Results obtained for a quiet day (2002, day 143) and for a stormy day (2002, day 350) are shown for the vertical (top) and for one horizontal component (E-W, bottom). Four hours of data (00–04 UTC) were used in the calculation. The quiet and the stormy day were selected on the basis of the spectral wave density (SWD) measured at the nearby NOAA buoy 46042. There were no significant earthquakes recorded during the two time periods.

[9] The MOBB vertical component data on a quiet day show a noise "hump" for periods between 20 and 200 s that is not present in the land station data. The observed peak at MOBB is even stronger and wider (periods 20–500 s) on a stormy day, when it can also be observed at the Farallon Islands station FARB. On the other hand, the noise at MOBB between 10 and 20 s is comparable to the quietest BDSN land stations. The results also show that the noise observed at MOBB on a quiet day for periods longer than 20 s is comparable to the noise observed at the island station on a stormy day. The sharp short-period cutoff observed at 20 s in the spectrum for the vertical MOBB component on a stormy day is determined by the water depth, since only linear waves with wave numbers comparable or smaller than the inverse of the water depth can generate a detectable pressure signal at the seafloor [Webb, 1998]. In the infragravity wave band, the difference between quiet and stormy period is larger at the lower frequencies than at the high-frequency end, with more low-frequency energy during storms.

[10] In the microseism band, the three peaks are evident between 1 and 10 s. They are often

observed in the spectra from the sites in the Pacific and are associated with the large storms in the Southern Ocean for the low-frequency peak, with the local storms in the North Pacific for the main peak, and with the local wind wave field for the high frequency peak [Webb, 1992, 1998]. On a stormy day, a well pronounced peak is present in the infragravity wave band between 20 and 30 s. A few more subtle peaks seem to be also present at longer periods within the infragravity wave band.

[11] The results for the two horizontal components were similar and therefore only one component (E-W) is shown in Figure 2. In this case there is no peak observed at MOBB for periods longer than 20 s on a quiet day. On the stormy day, the increased noise at MOBB is present again. The signal at the island station FARB is even stronger than at MOBB and it extends all the way to 1000 s.

[12] The shape of the noise spectra in the infragravity wave band measured at MOBB is in agreement with observations from previous deployments in which seismometers were buried under the ocean floor [Stephen et al., 2003; Araki et al., 2004], as well as with theoretical predictions [Araki et al., 2004].

4. Generation of Infragravity Waves

[13] We computed PSD for 1-hour long segments for all the available MOBB data until July 2004 and compared the results to the SWD measured at the nearby NOAA buoys. The SWD is computed at the buoys once every hour and it measures energy of the ocean waves in m^2/Hz in the 0.01 Hz wide frequency bins that cover the 0.03 to 0.4 Hz range. The location of the buoys considered is shown in Figure 3. Comparison spectrograms for a 7-day period (12/9–16/2003) are presented in Figure 4. The infragravity peak can be observed in the PSD plot for the vertical MOBB channel throughout the 7-day period (Figure 4, top panel). A rather sudden change of the infragravity peak width is indicated with a black line. The second panel from top in Figure 4 shows the SWD measured at the western most buoy 46059, and the panels below the SWD at three other nearshore buoys ordered by longitude. The storm observed on day 344 was approaching from the WNW direction, as the mean wave direction corresponding to energy of the dominant period measured at buoy 46042 in the second half of day 344 ranged from 280° to 295° from North. Increased energy of the 10–20 s ocean
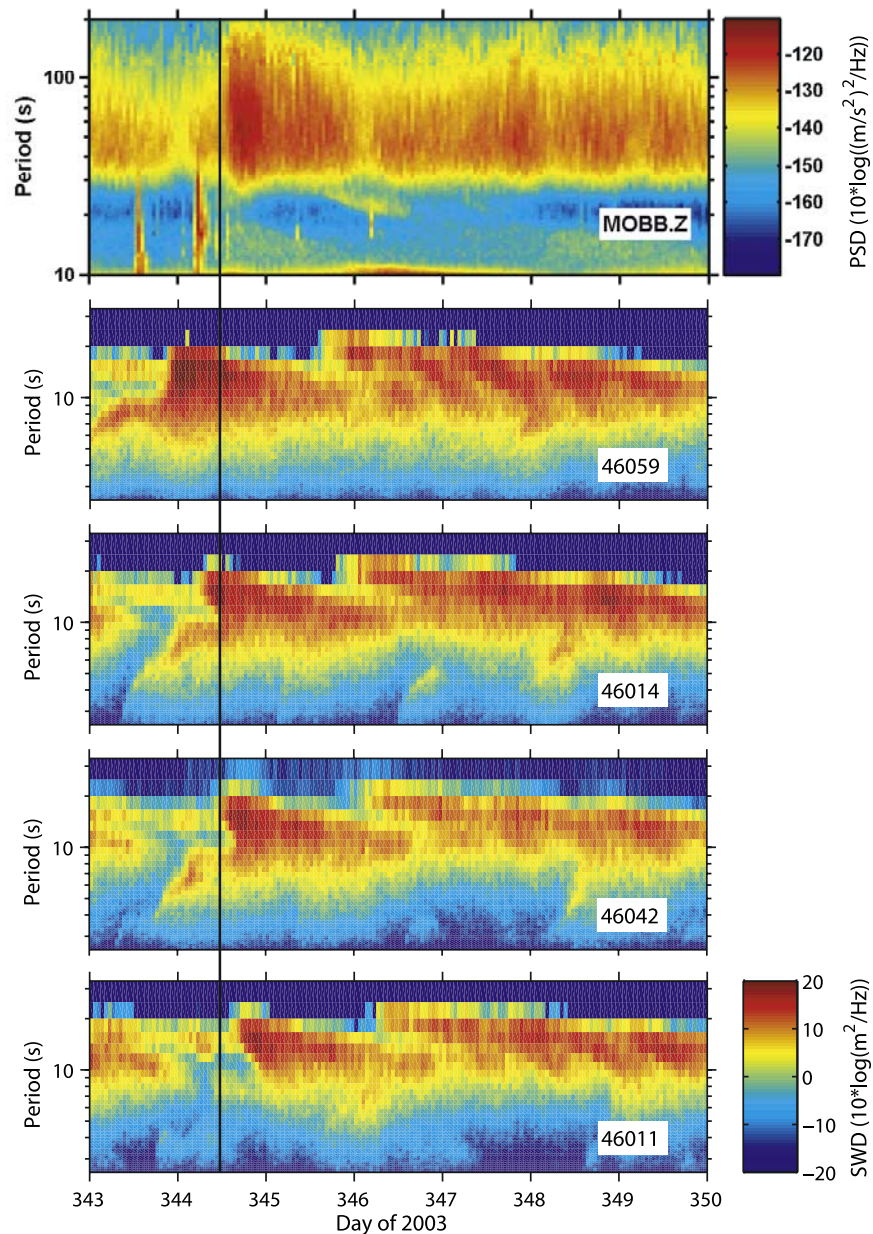
Figure 4. Top panel shows the power spectral density (PSD) for the vertical MOBB channel as a function of period and time. Bottom panels show the spectral wave density (SWD) calculated at 4 buoys. The vertical line indicates a sudden change of the infragravity peak width.

waves on day 344 can therefore first be seen on buoy 46059, and last on buoy 46011. The arrival of these waves at buoy 46042 coincides with the increase of the infragravity signal on MOBB. Buoy 46042 is the closest one to MOBB, located only 23 km to the W (see Figure 1). The fact that the arrival of the ocean waves coincides with increase of the infragravity signal clearly tells us that the infragravity waves observed at MOBB during this time period are primarily locally generated. The same can generally be observed

throughout the deployment and for storms arriving from different azimuths.

[14] The narrow peaks observed between 10 and 40 s in the second half of day 343 and early on day 344 correspond to an Mw 6.2 Andreanof Islands (Aleutian Islands) earthquake and to an Mw 6.8 earthquake in Taiwan. We also see a dispersed swell arrival with 18–26 s periods between days 345 and 347. We followed the approach described in *Bromirski and Duennebier* [2002] and inverted
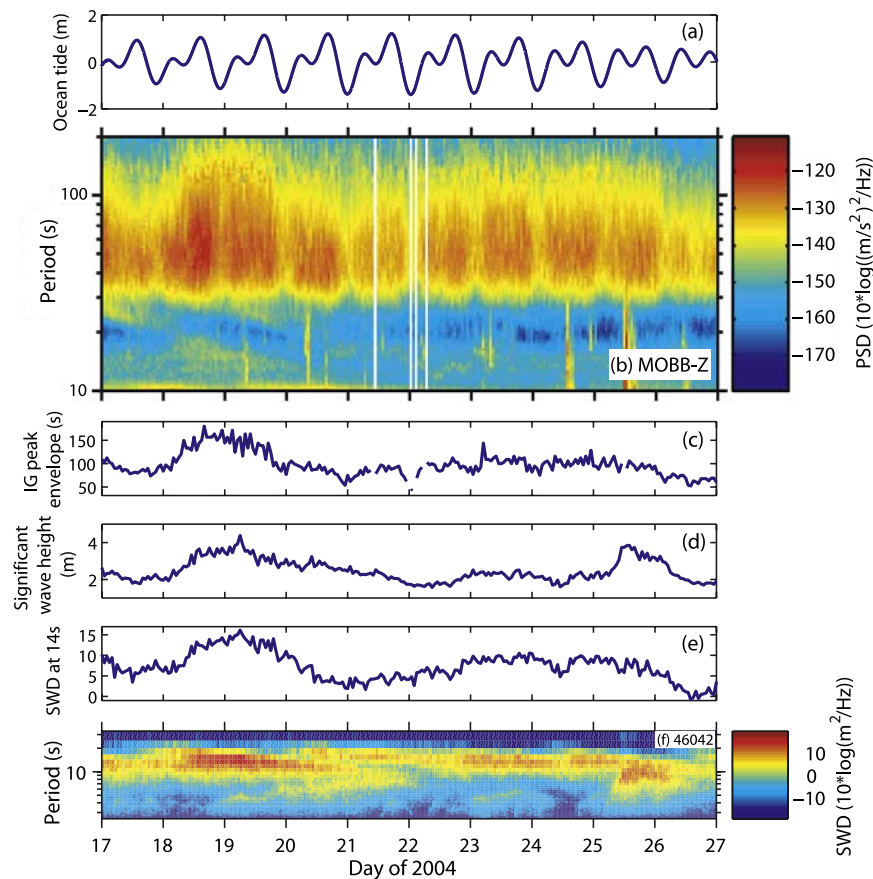
Figure 5. (a) Theoretical ocean tide at the MOBB location. (b) The power spectral density (PSD) for the vertical MOBB channel as a function of period and time. White lines indicate hours with some missing data. (c) The envelope of the infragravity peak presented in Figure 5b, taken at the long-period end, at the PSD value of −136 dB. (d) The significant wave height at the buoy 46042. (e) The spectral wave density (SWD) in the 14.3 s period bin at the buoy 46042. (f) The SWD at the buoy 46042.

the dispersion trend to obtain the origin time and distance to the swell source. We assumed a mean water depth of 4500 m along the swell propagation path and obtained a distance of 4800 km and for the origin time, 01 UTC on day 343. By comparing the SWD from the buoys in the Pacific Ocean around the calculated origin time, we matched the swell source to a strong storm observed at the buoy 46072, located in the central Aleutians, 4233 km from MOBB. Similar dispersed swell arrivals can often be observed at MOBB and most of the time their origin can be traced to the northern or northeastern Pacific Ocean.

5. Modulation of Infragravity Signal

[15] The PSD for the vertical MOBB component for a 10-day period (01/17–27/2004) is shown in Figure 5b. As before, the strongest infragravity signal (days 18–20) coincides with the increased

energy of 10–20 s ocean waves as recorded at the local buoy 46042 (Figure 5f), although the arrival of the storm is not as sharp as in the previous example. In addition, two types of modulation of the infragravity peak can be observed.

[16] The modulation with a period equal to the diurnal tide and to a lesser extent the semidiurnal tide is best seen at the short-period end of the infragravity peak (30–40 s periods) as well as throughout the entire infragravity band. It can be observed for the entire 10-day period. In fact, modulation as described below is observed throughout the deployment. This modulation clearly correlates with the amplitude of the ocean tides at MOBB, shown in Figure 5a. Comparison of the PSD and the tides shows that the infragravity waves have less energy at low tides. This can best be seen for the strongest minima in tides that occur close to the beginning of each day for this time period. Additional small modula-
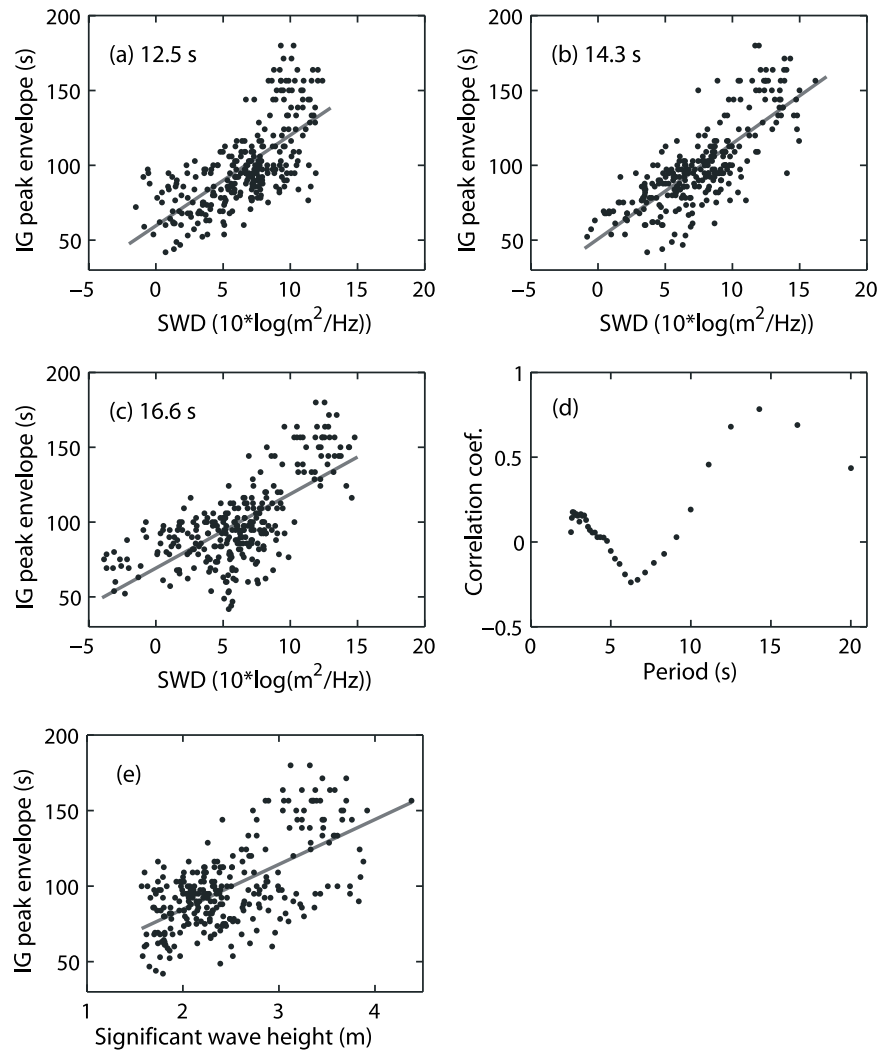
Figure 6. (a–c) The period of the infragravity peak envelope, taken at the long-period end, at the PSD value of −136 dB, as a function of the SWD observed at buoy 46042 in the 12.5, 14.3, and 16.6 s period bins. (d) The correlation coefficient between the period of the infragravity peak envelope and the SWD observed in the individual bins at buoy 46042, as a function of the SWD bin period. (e) The period of the infragravity peak envelope as a function of the significant wave height as observed at the buoy 46042. Gray lines show best linear fits to the data.

tion can also be seen, particularly at the short-period end of the infragravity peak. It coincides with the second strongest tides minima which occur close to the middle of the day for this time period.

[17] Also observed is a low-frequency modulation which is best seen as the variation of the period on the long-period side of the infragravity peak at which the infragravity peak rises above the noise from other sources (Figures 5b and 5c). The envelope of the observed infragravity peak on the long-period side was taken at the PSD value of −136 dB. The infragravity peak extends to longest periods during days 18 and 19, and then again slightly increases between days 22 and 26. First we

compare this to the significant wave height measured at the local buoy 46042 (Figure 5d). Significant wave height is the average of the highest 1/3 of all of the wave heights during the 20-minute sampling period, calculated once every hour. The two agree well in the first half of the 10-day period, but then significant wave height has a peak in the second half of the day 25. Comparison with the SWD plot (Figure 5f) reveals that at that time most of the wave energy was in the waves with periods shorter than 10 s. We therefore looked at the correlation between the period of the infragravity peak envelope and the wave energy in individual frequency bins as observed at the local buoy. The best correlation was observed with the ocean
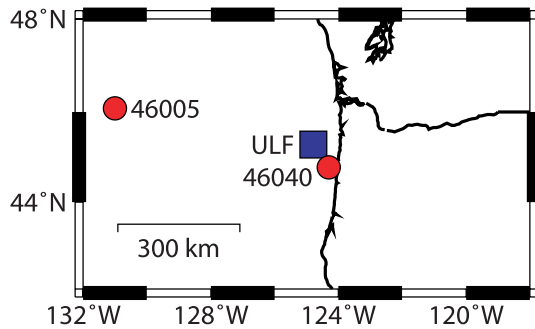
Figure 7. The location of the Oregon ULF station and the two closest NOAA buoys that had spectral wave density data available for the time period of the Oregon ULF/VLF experiment.

waves with 14.3 s period for which the SWD is shown in Figure 5e and Figure 6b. Correlations between the period of the infragravity peak envelope and SWD of the ocean waves at two other periods (12.5 s and 16.6 s) as well as the significant wave height are also shown in Figure 6. The correlation coefficient between the period of the infragravity peak envelope and the SWD observed in the individual bins at buoy 46042, as a function of the SWD bin period, is presented in Figure 6d, and confirms that the infragravity peak long-period modulation correlates the strongest with the ocean wave energy at ∼14 s.

6. Observation of Infragravity Signal During the Oregon ULF/VLF Experiment

[18] We have performed a similar analysis with the seismic and buoy data recorded during the

Oregon ULF/VLF temporary deployment in 1991 [*Bromirski and Duennebier*, 1995, 2002]. In this experiment the seismic data were recorded at the 3-component Guralp CMG-3 broadband seismometer, sensitive from 50 Hz to 0.01 Hz (100 s), that was buried in the ocean floor, about 48 km off the Oregon coast (Figure 7). The water depth at this location was about 600 m. The locations of the two closest NOAA buoys that had spectral wave density data available for the time period of the experiment are shown in Figure 7. The closer buoy 46040 was located 68 km SSE of the seismometer location, at the water depth of 112 m, and about 20 km from the coast. The deepwater buoy 46005 was located 493 km W of the seismometer location.

[19] In Figure 8, the PSD at the Oregon ULF station for a 4-hour period on a quiet day (1999, day 200, 07–11 UTC) is compared to the PSD on a stormy day (1999, day 205, 06–10 UTC). There were no significant earthquakes recorded during the two time periods. The results obtained for the vertical component show that the infragravity peak can be observed in the PSD during both quiet and stormy periods. The vertical component data on a quiet day show a noise "hump" for periods between 16 and 115 s. The observed peak is stronger on a stormy day. Since the noise level around the infragravity peak is also much higher on a stormy day, the short- and long-period ends of the infragravity peak are hidden and cannot be directly compared to the ones observed on a quiet day. At Oregon ULF, the infragravity "hump" cannot be observed on either of the two horizontal components, although results for only one are shown in Figure 8. This indicates that for the
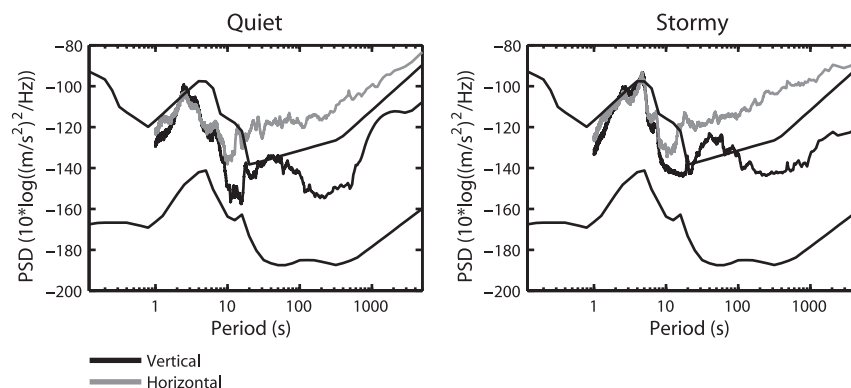

Figure 8. Comparison of the power spectral density (PSD) at the Oregon ULF station for a quiet day (1999, day 200, 07–11 UTC) and for a stormy day (1999, day 205, 06–10 UTC). Results obtained for the vertical (black) and for the horizontal component that was rotated 176.3° from North (gray) are shown. The USGS high- and low-noise models for land stations are shown as thin black lines [*Peterson*, 1993].
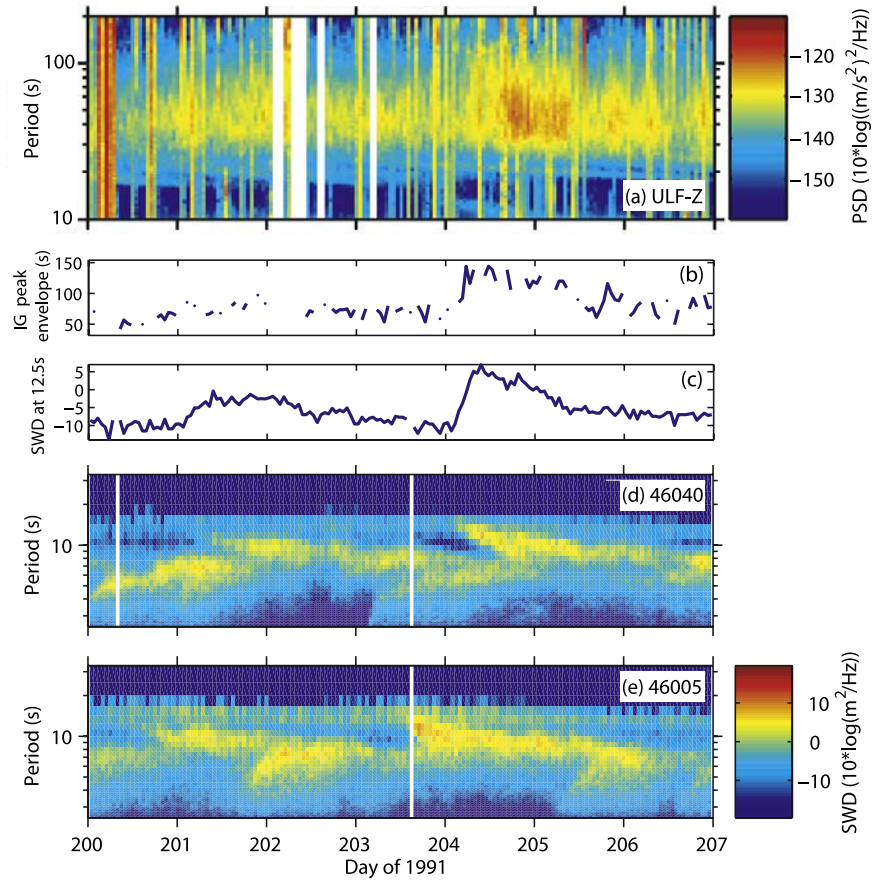
Figure 9. (a) The power spectral density (PSD) for the Oregon ULF vertical channel as a function of period and time. White lines indicate hours with some missing data. (b) The envelope of the infragravity peak presented in Figure 9a, taken at the long-period end, at the PSD value of -136 dB. (c) The spectral wave density (SWD) in the 12.5 s period bin at the buoy 46040. (d) The SWD at the buoy 46040. (e) The SWD at the buoy 46005.

horizontal components, noise sources other than infragravity waves are dominant at periods longer than 10 s. Part of this noise is probably generated by slight movements of the buried seismic package [*Bromirski and Duennebier*, 1995].

[20] When compared to the result obtained with the MOBB data, the short-period end of the infragravity peak observed for the vertical component data extends to shorter periods. This is expected as the Oregon ULF station was located at only 600 m water depth. The pressure signal at the seafloor of depth H is related to the surface wave height ζ by

$$P_{bottom} = \rho g\zeta / \cosh(kH) \approx P_{surface} e^{-kH}, \qquad (1)$$

where k is the wave number and ρ is water density. Assuming that the pressure fluctuations are caused by freely traveling surface gravity waves the

dispersion relation can be used to determine the wave number

$$\omega^2 = gk \tanh(kH), \qquad (2)$$

where ω is angular frequency of the ocean gravity wave. For water depth at MOBB H = 1000 m and $\omega = 2\pi/20s$, which corresponds to the observed short-period cutoff period at MOBB, we obtain the value for the product of the wave number and water depth kH = 10.1. Using equation (2) for water depth H = 600 m and kH = 10.1 from the above MOBB example, we obtain the expected short-period cutoff period for the Oregon experiment to be 15.5 s. This agrees well with the observed short-period cutoff value of 16 s.

[21] The seismic data from the Oregon experiment are noisier than the MOBB data presented above, but the infragravity signal can still easily be ob-
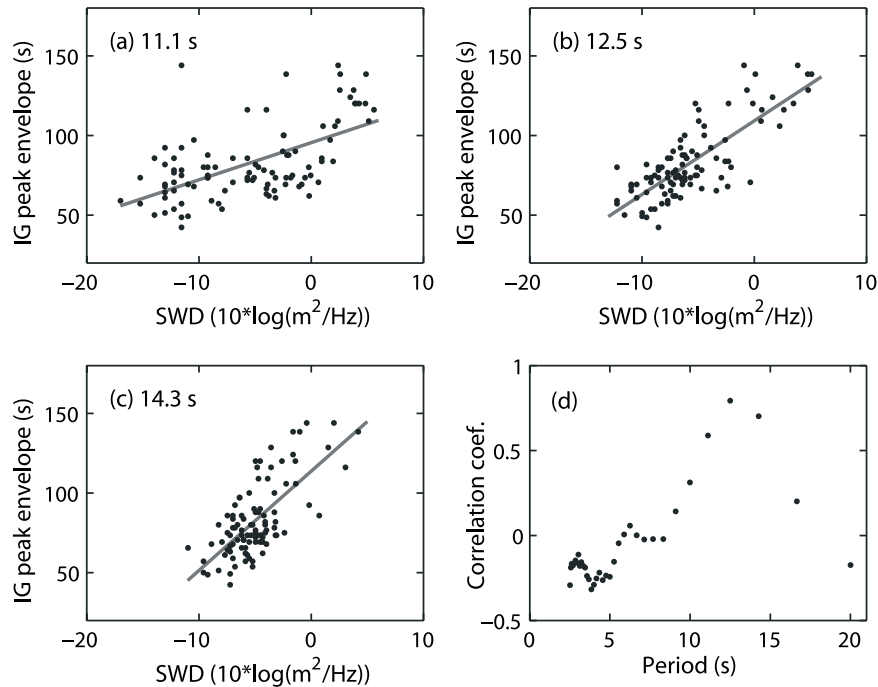
Figure 10. (a–c) The period of the infragravity peak envelope, taken at the long-period end, at the PSD value of −136 dB, as a function of the SWD observed at buoy 46040 in the 11.1, 12.5, and 14.3 s period bins. Gray lines show best linear fits to the data. (d) The correlation coefficient between the period of the infragravity peak envelope and the SWD observed in the individual bins at buoy 46040, as a function of the SWD bin period.

served during the 7-day deployment period (7/19–26/1991; Figure 9a). The SWD recorded at the two buoys is shown in Figures 9d and 9e. The signal recorded at the local buoy 46040 is again better correlated with the seismic PSD. The increased infragravity signal observed between days 204 and 206 matches the arrival of the 10–20 s ocean waves as recorded on the local buoy 46040.

[22] The low-frequency modulation of the infragravity peak can again be seen as the variation of the period on the long-period side of the infragravity peak at which the infragravity peak rises above the noise from other sources (Figures 9a and 9b). The envelope of the observed infragravity peak on the long-period side was taken at the PSD value of −136 dB. The hours that had increased noise throughout the 10–200 s period band were not used in the calculation. The correlation between the period of the infragravity peak envelope and the wave energy in individual frequency bins as observed at the local buoy 46040 is presented in Figure 10. The best correlation was observed with the ocean waves with 12.5 s period for which the SWD is shown in Figure 9c and Figure 10b. Correlations between the period of the infragravity peak envelope and SWD of the ocean waves at two other periods (11.1 s and 14.3 s) are shown in

Figures 10a and 10c. The correlation coefficient between the period of the infragravity peak envelope and the SWD observed in the individual bins at buoy 46040, as a function of the SWD bin period, is presented in Figure 10d, and confirms that the infragravity peak long-period modulation correlates the strongest with the ocean wave energy at ~12.5 s.

7. Discussion

7.1. Tidal Modulation of the Infragravity Signal

[23] The fact that the observed modulated infragravity signal is weakest at low tides is just the opposite from what one would expect from hydrodynamic filtering. The term "hydrodynamic filtering" is often used to describe that the pressure signal from the ocean waves decays exponentially with water depth, depending on the wave number of the waves [Kinsman, 1984]. Since only linear waves with wave numbers comparable or smaller than the inverse of the water depth can generate detectable pressure fluctuations at the seafloor, one would expect that the higher water column above MOBB at high tides would shield it against pres-

sure signal from the higher frequency infragravity waves, which would result in weaker signal. What we observe is just the opposite which indicates that the tides must play an important role in the generation of the infragravity waves rather than just weakening the pressure signal at the ocean bottom. Also, the effect of the hydrodynamic filtering due to only a few meters high tides in a 1000 m water depth is very small. Using equation (1), the relative change in the pressure variation at the bottom due to 3 m water depth variation can be estimated to be only about 6% for k = 0.01/m (λ = 324 m). In addition, such changes in hydrodynamic filtering should have stronger effect on the shorter-period infragravity waves. Our observations, on the other hand, show that strong modulation can be observed throughout the entire infragravity band.

[24] Previous studies of the nonlinear interaction between short-period waves and currents [*Longuet-Higgins and Stewart*, 1960, 1961, 1964] found that the energy variations of the short-period waves correspond to work done by the currents against the radiation stress of the short-period waves. The magnitude of the energy exchange between the short-period waves and tidal current depends on the pattern of the tidal currents, but in simple situations, the energy of the short-period waves is in phase with the tidal elevations [*Longuet-Higgins and Stewart*, 1964]. This agrees with our observations. At the moment, currents are not measured at the nearby NOAA buoys, but the currents observed at the ocean bottom at MOBB clearly show the tidal pattern [*Romanowicz et al.*, 2005, Figure 9; *Uhrhammer et al.*, 2003]. Since the current direction and speed at shallow water depths as well as direction and amplitude of the incoming short-period waves all influence the efficiency of the energy exchange during nonlinear interaction between short-period waves and currents, future modeling of the observations at MOBB will help us better understand the underlying processes. For this purpose a better knowledge of the surface currents is needed.

[25] Another effect that the tides have on the generation of the infragravity waves is through different topography that is brought into play at the same water depth during different tide heights. A study by *Herbers et al.* [1995b] observed that the energy levels of the free infragravity waves on the shelf depend on the surrounding topography. They suggested that the shelf topography is important to the propagation and trapping of free infragravity motions and that generation and reflection of free

infragravity waves is sensitive to the shoreline morphology. In our case the topography around MOBB is very complex (see Figure 1) and it is possible that already a small water depth change can significantly perturb the conditions for generation and reflection of infragravity waves. Our observations seem to agree with observations by *Herbers et al.* [1995b], as we record stronger infragravity signal at high tides, when the shelf is slightly wider. Since MOBB is located close to the edge of the shelf our results suggest that at high tides infragravity waves are more efficiently generated on the shelf and/or can more efficiently leak from the shelf into the deeper water. Previous studies that observed tidal modulation of the infragravity energy close to shore [e.g., *Guza and Thornton*, 1982; *Okihiro and Guza*, 1995] suggested that tidal modulation could result either from the changes of the beach face slope with the tides or the changes of the surf zone width.

7.2. Short-Period (12–14 s) Ocean Wave Energy Modulation of the Infragravity Signal

[26] The low-frequency modulation of the observed infragravity signal during a 10-day stormy period at MOBB is best correlated with the energy of the 14.3 s period ocean waves. A similar result can be obtained for other stormy periods at MOBB. Analysis of the data recorded during the Oregon ULF/VLF experiment shows best correlation with the energy of the slightly shorter, 12.5 s period ocean waves. The data from the Oregon experiment only span over a 7-day period in which the energy of the ocean waves was significantly lower than during the time period used for MOBB. Also, the sensor used in the Oregon experiment had a shorter long-period corner frequency. We believe that for a better understanding of the influence of the water depth and regional topography on the observed correlation between the period of the ocean waves and the low-frequency modulation of the infragravity peak, data from stations deployed simultaneously and in a relative proximity of each other, as well as equipped with seismometers sensitive to longer than 100 s periods, should be used. Nevertheless, the results from both deployments are telling us that the modulation of the short-period (12–14 s) ocean wave energy can be observed in the infragravity signal as well. This suggests that the short-period ocean waves are essential for the generation of the infragravity waves. It is interesting to note that the same period ocean waves are also the source of the microseisms

noise, observed at the double frequency, at 6–7 s. This suggests that the generation mechanisms of infragravity waves and double frequency microseisms are closely related, and originate from the non-linear interaction of ~14 s ocean waves, as already well documented for the microseisms [e.g., *Longuet-Higgins*, 1950].

7.3. Future Work

[27] In addition to the results presented in this paper we have done a preliminary investigation of the data recorded at the station KEBB, located offshore Washington, at a water depth of 2376 m. Station KEBB is part of the NEPTUNE project whose goal is to establish a regional ocean observatory in the northeast Pacific Ocean. Preliminary results showed that infragravity waves observed at station KEBB were mainly generated close to the nearby coast. A number of buoys as well as additional ocean bottom broadband seismometers that are already installed in the region, but for which the data are not available yet, will be used to learn more about the directional properties of the observed infragravity waves. This will be the subject of our future study.

8. Conclusions

[28] The primary reason for installing ocean bottom broadband seismic stations is to record earthquakes. Any other signal is often regarded as noise and additional processing is required to remove it (D. Dolenc et al., manuscript in preparation, 2005). At the same time observations of non-seismic signals, like infragravity waves, can help us learn more about their generation and propagation. Such observations can also enable us to better understand the coupling between the ocean and the solid earth and learn more about the earth structure using non-seismic sources.

[29] Infragravity waves can be observed at the permanent ocean bottom broadband seismic station MOBB on stormy as well as quiet days. When compared to the energy of the short-period ocean waves recorded at the local buoys, infragravity waves in the longer than 20 s period band are found to be mainly locally generated from shorter-period waves. Two types of modulation of the infragravity signal are observed. First, the entire infragravity band is modulated in-phase with tides. It is possible that this is a result of the nonlinear exchange of energy between the short-period waves and tidal currents. Second,

the low-frequency modulation of the observed infragravity peak is best correlated with the energy of the 14.3 s period ocean waves, suggesting a close relation of infragravity wave generation to that of double frequency microseisms, which have maximum energy at 6–7 s. Analysis of the data recorded during the Oregon ULF/VLF experiment also indicates that infragravity waves are primarily locally generated. In this case, the low-frequency modulation of the observed infragravity peak is best correlated with the energy of the 12.5 s period ocean waves. To better understand the influence of the water depth and regional topography on the observed correlation between the low-frequency modulation of the infragravity peak and period of the ocean waves it would be important to use data from stations deployed simultaneously in a relative proximity of each other.

[30] To better understand the coupling between the ocean and the solid earth it will be important to compare observations from different broadband ocean bottom stations and nearby buoys. Future experiments that will include a large array of ocean bottom broadband seismometers as well as data from a dense network of ocean buoys will help us learn more about the directional distribution of infragravity waves and their generation.

Acknowledgments

References

Agnew, D. C. (1996), SPOTL: Some programs for ocean-tide loading, *SIO Ref. Ser.*, *96-8*, 35 pp., Scripps Inst. of Oceanogr., La Jolla, Calif.

Araki, E., M. Shinohara, S. Sacks, A. Linde, T. Kanazawa, H. Shiobara, H. Mikada, and K. Suyehiro (2004), Improvement of seismic observation in the ocean by use of seafloor boreholes, *Bull. Seismol. Soc. Am.*, *94*, 678–690.

Bromirski, P. D., and F. K. Duennebier (1995), Seismoacoustic signals and noise in the near-shore environment, *SOEST Rep. 95-03*, 110 pp., Univ. of Hawaii, Honolulu.

Bromirski, P. D., and F. K. Duennebier (2002), The near-coastal microseism spectrum: Spatial and temporal wave climate relationships, *J. Geophys. Res.*, *107*(B8), 2166, doi:10.1029/2001JB000265.

Cox, C., T. Deaton, and S. Webb (1984), A deep-sea differential pressure gauge, *J. Atmos. Oceanic Technol.*, *1*, 237–246.

Elgar, S., T. H. C. Herbers, M. Okihiro, J. Oltman-Shay, and R. T. Guza (1992), Observations of infragravity waves, *J. Geophys. Res.*, *97*, 15,573–15,577.

Guza, R. T., and E. B. Thornton (1982), Swash oscillations on a natural beach, *J. Geophys. Res.*, *87*, 483–492.

Herbers, T. H. C., S. Elgar, and R. T. Guza (1995a), Generation and propagation of infragravity waves, *J. Geophys. Res.*, *100*, 24,863–24,872.

Herbers, T. H. C., S. Elgar, R. T. Guza, and W. C. O'Reilly (1995b), Infragravity-frequency (0.005–0.05 Hz) motions on the shelf, Part II: Free waves, *J. Phys. Oceanogr.*, *25*, 1063–1079.

Kinsman, B. (1984), *Wind Waves: Their Generation and Propagation on the Ocean Surface*, 676 pp., Prentice-Hall, Upper Saddle River, N. J.

Longuet-Higgins, M. S. (1950), A theory of the origin of microseisms, *Philos. Trans. R. Soc. London, Ser. A*, *243*, 1–35.

Longuet-Higgins, M. S., and R. W. Stewart (1960), Changes in the form of short gravity waves on long waves and tidal currents, *J. Fluid Mech.*, *8*, 565–583.

Longuet-Higgins, M. S., and R. W. Stewart (1961), The changes in amplitude of short gravity waves on steady non-uniform currents, *J. Fluid Mech.*, *10*, 529–549.

Longuet-Higgins, M. S., and R. W. Stewart (1964), Radiation stresses in water waves: A physical discussion, with applications, *Deep Sea Res. Oceanogr. Abstr.*, *11*, 529–562.

McGill, P., D. Neuhauser, D. Stakes, B. Romanowicz, T. Ramirez, and R. Uhrhammer (2002), Deployment of a long-term broadband seafloor observatory in Monterey Bay, *Eos Trans. AGU*, *83*(47), Fall Meet. Suppl., Abstract S71A-1049.

Munk, W. H. (1949), Surf beats, *Eos Trans. AGU*, *30*, 849–854.

Okihiro, M., and R. T. Guza (1995), Infragravity energy modulation by tides, *J. Geophys. Res.*, *100*, 16,143–16,148.

Peterson, J. (1993), Observation and modeling of seismic background noise, *U.S. Geol. Surv. Tech. Rep.*, *93-322*, 95 pp.

Rhie, J., and B. Romanowicz (2004), Excitation of Earth's continuous free oscillations by atmosphere-ocean-seafloor coupling, *Nature*, *431*, 552–556.

Romanowicz, B., et al. (1998), MOISE: A pilot experiment towards long term sea-floor geophysical observatories, *Earth Planets Space*, *50*, 927–937.

Romanowicz, B., D. Stakes, R. Uhrhammer, P. McGill, D. Neuhauser, T. Ramirez, and D. Dolenc (2003), The MOBB Experiment: A prototype permanent off-shore ocean bottom broadband station, *Eos Trans. AGU*, *84*(34), 331–332, 325.

Romanowicz, B., D. Stakes, D. Dolenc, D. Neuhauser, P. McGill, R. Uhrhammer, and T. Ramirez (2005), The Monterey Bay broadband ocean bottom seismic observatory, *Ann. Geophys.*, in press.

Snodgrass, F. E., G. W. Groves, K. F. Hasselmann, G. R. Miller, W. H. Munk, and W. H. Powers (1966), Propagation of ocean swell across the Pacific, *Philos. Trans. R. Soc. London, Ser. A*, *259*, 431–497.

Stephen, R. A., F. N. Spiess, J. A. Collins, J. A. Hildebrand, J. A. Orcutt, K. R. Peal, F. L. Vernon, and F. B. Wooding (2003), Ocean Seismic Network Pilot Experiment, *Geochem. Geophys. Geosyst.*, *4*(10), 1092, doi:10.1029/2002GC000485.

Stutzmann, E., et al. (2001), MOISE: A prototype multiparameter ocean-bottom station, *Bull. Seismol. Soc. Am.*, *91*, 885–892.

Sutton, G. H., W. G. McDonald, D. D. Prentiss, and S. N. Thanos (1965), Ocean-bottom seismic observatories, *Proc. IEEE*, *53*, 1909–1921.

Tanimoto, T. (2005), The oceanic excitation hypothesis for the continuous oscillation of the Earth, *Geophys. J. Int.*, *160*, 276–288.

Tucker, M. J. (1950), Surf beats: Sea waves of 1 to 5 min. period, *Proc. R. Soc. London, Ser. A*, *202*, 565–573.

Uhrhammer, R., B. Romanowicz, D. Neuhauser, D. Stakes, P. McGill, and T. Ramirez (2002), Instrument testing and first results from the MOBB Observatory, *Eos Trans. AGU*, *83*(47), Fall Meet. Suppl., Abstract S71A-1048.

Uhrhammer, R. A., D. Dolenc, B. Romanowicz, D. Stakes, P. McGill, D. Neuhauser, and T. Ramirez (2003), MOBB: Data analysis from an ocean floor broadband seismic observatory, *Eos Trans. AGU*, *84*(46), *Fall Meet. Suppl.*, Abstract S52D-0162.

Webb, S. C. (1992), The equilibrium microseism spectrum, *J. Acoust. Soc. Am.*, *92*, 2141–2158.

Webb, S. C. (1998), Broadband seismology and noise under the ocean, *Rev. Geophys.*, *36*, 105–142.

Webb, S. C., X. Zhang, and W. Crawford (1991), Infragravity waves in the deep ocean, *J. Geophys. Res.*, *96*, 2723–2736.